Journal of Materials Chemistry A

PAPER

View Article Online
View Journal | View Issue

Cite this: J. Mater. Chem. A, 2016, 4, 5917

On the relationship between chemical expansion and hydration thermodynamics of proton conducting perovskites

Tor S. Bjørheim,* Andreas Løken and Reidar Haugsrud

In this contribution, we determine the compositional dependence of the chemical expansion and entropy of hydration of the proton conducting perovskites $BaZrO_3$, $BaSnO_3$, $BaCeO_3$, and $SrZrO_3$ by first principles phonon calculations. The calculations reveal that the cubic $BaZrO_3$ and $BaSnO_3$, which display the *least favourable* hydration enthalpies, −72 and −65 kJ mol^{-1}, respectively, exhibit the *most favourable* entropies, −108 and −132 J mol^{-1} K^{-1}, respectively. The strong compositional dependency of the hydration entropy primarily originates from the entropy gain upon filling the oxygen vacancy, which is closely related to the chemical expansion coefficient of oxygen vacancies, and thus the chemical expansion upon hydration. The chemical expansion coefficient of oxygen vacancies is more negative for the cubic than the orthorhombic perovskites, leading to a considerably larger chemical expansion upon hydration of the former. The calculations therefore suggest that challenges associated with chemical expansion upon hydration of $BaZrO_3$ proton conducting electrolytes to some extent can be avoided, or reduced, by partial substitution of Zr by Ce.

Received 10th December 2015
Accepted 26th February 2016

DOI: 10.1039/c5ta10090a

www.rsc.org/MaterialsA

1 Introduction

Protons dissolve in many oxides[1] through hydration of oxygen vacancies, resulting in high temperature proton conduction with potentials for important applications such as in fuel cells and gas separation membranes. The relative dominance of protons and oxygen vacancies is determined by the *enthalpy* and *entropy* of the hydration reaction

$$H_2O(g) + O_O^{\times} + v_O^{\bullet\bullet} \leftrightharpoons 2OH_O^{\bullet}, \quad (1)$$

with the corresponding equilibrium constant:

$$K_{Hydr} = \frac{\left(c_{OH_O^{\bullet}}\right)^2}{c_{v_O^{\bullet\bullet}}\ c_{O_O^{\times}} p_{H_2O}} = \exp\left(\frac{\Delta_{Hydr}S^{\circ}}{R}\right)\exp\left(-\frac{\Delta_{Hydr}H^{\circ}}{RT}\right) \quad (2)$$

where c_i are the molar concentrations of protons, oxygen vacancies, and lattice oxygen species. The enthalpy of this reaction can be evaluated by both indirect[2] and direct measurements,[3–5] or computationally, and correlates with various materials' parameters.[5–9] The entropy on the other hand, has never been measured directly, and its nature and compositional dependence is in general poorly understood. We recently determined $\Delta_{Hydr}S^{\circ}$ of $BaZrO_3$ computationally,[10] and revealed that its major contribution is the vibrational entropy of oxygen vacancies ($v_O^{\bullet\bullet}$), in addition to loss of water vapour. Although the vibrational contribution from protons was found to be small, there is a significant configurational contribution due to their site degeneracy around the oxide ions in the perovskite structure. In this contribution, we continue our efforts to understand the entropy of hydration, by for the first time assessing its compositional dependence and relationship with the chemical expansion, computationally.

$\Delta_{Hydr}H^{\circ}$ has been shown to correlate with material specific parameters such as the difference in the electronegativity of the B- and A-site cations[8] and the tolerance factor,[9] which has been argued to reflect its dependence on the basicity, or partial charge density of the oxide ions.[7,11] $\Delta_{Hydr}S^{\circ}$, however, seemingly does not display any similar correlations,[8] which partly may stem from the large scatter in the experimental range of values. Further, the compositional dependence of $\Delta_{Hydr}S^{\circ}$ is less intuitive than that of $\Delta_{Hydr}H^{\circ}$ as it is related to both the chemical expansion of the material upon $v_O^{\bullet\bullet}$ and $OH_O^{\bullet}$ formation, the bonding strengths of H^+ and O^{2-}, and the local structural relaxations induced by the two defects.

To assess the compositional and structural dependency of $\Delta_{Hydr}S^{\circ}$, we evaluate the vibrational formation entropies of $v_O^{\bullet\bullet}$ and $OH_O^{\bullet}$ from first principles phonon calculations, and the configurational contribution originating from the site degeneracy of protons (and oxygen vacancies). We have chosen to focus on four structurally different proton conducting perovskites; $BaZrO_3$, $BaSnO_3$, $BaCeO_3$ and $SrZrO_3$. The two former take on a cubic structure ($Pm\bar{3}m$), while the two latter adopt an orthorhombic structure (*Pnma*), thus allowing us to judge the effect of both symmetry and composition on $\Delta_{Hydr}S^{\circ}$. As shown

Centre for Materials Science and Nanotechnology, Department of Chemistry, University of Oslo, FERMiO Gaustadalléen 21, 0349 Oslo, Norway. E-mail: torsb@kjemi.uio.no

Table 1 Selected experimentally determined hydration enthalpies ($\Delta_{Hydr}H^\circ$) and entropies ($\Delta_{Hydr}S^\circ$) of acceptor doped $BaZrO_3$, $BaSnO_3$, $BaCeO_3$ and $SrZrO_3$

	$\Delta_{Hydr}H^\circ$ (kJ mol^{-1})	$\Delta_{Hydr}S^\circ$ (J mol^{-1} K^{-1})
$BaZrO_3$		
10 mol% Y[6]	−80	−89
$BaSnO_3$		
5 mol% Y[12]	−46	−95
12.5 mol% Y[12]	−50	−88
12.5 mol% Y[13]	−59	−97
$BaCeO_3$		
10 mol% Y[2]	−162	−167
10 mol% Y[11]	−135	−141
$SrZrO_3$		
5 mol% Yb[14]	−106	−127

in Table 1, the experimental $\Delta_{Hydr}H^\circ$ and $\Delta_{Hydr}S^\circ$ for these perovskites cover a wide range of values, with the cubic $BaZrO_3$ and $BaSnO_3$ exhibiting the least exothermic $\Delta_{Hydr}H^\circ$, but also the least negative (most favourable) $\Delta_{Hydr}S^\circ$.

First principles phonon calculations allow us to determine both $\Delta_{Hydr}H^\circ$ and $\Delta_{Hydr}S^\circ$ as a function of temperature, and explore the individual contributions that constitute both thermodynamic parameters. The calculations are performed under constant volume and/or constant/zero pressure conditions, in order to separate contributions from local relaxations and chemical expansion to the vibrational entropies.

2 Thermodynamic formalism

2.1 Defect formation thermodynamics

The free energy of defect formation, $\Delta_F F_{defect}$ (or $\Delta_F G_{defect}$) is given by

$$\Delta_F F_{defect} = \Delta E^{el}_{defect} + \Delta_F F^{vib}_{defect} + \sum_1^i \Delta n_i \mu_i(T,p) \; + q(\varepsilon_f + \Delta\varepsilon) \tag{3}$$

where ΔE^{el}_{defect} is the total energy difference between the defective and perfect supercells, while $\Delta_F F^{vib}_{defect}$ is the vibrational (phonon) contribution to the formation energy. Further, Δn_i is the change in the number of atoms i with chemical potential μ_i, q is the effective charge of the defect, ε_f is the Fermi level and $\Delta\varepsilon$ aligns the core potentials of the perfect and the defective supercells to remedy shifts in the band edges due to the jellium background charge. The chemical potential of H_2O is given by

$$\mu_{H_2O} = \overset{\circ}{\mu}_{H_2O} + H^{zp}_{H_2O} + \overset{\circ}{H}_{H_2O}(T) - T\overset{\circ}{S}_{H_2O}(T) + k_B T \ln\left(\frac{p_{H_2O}}{p^\circ}\right) \tag{4}$$

where the zero-point energy ($H^{zp}_{H_2O}$), is obtained from the calculated vibrational frequency of a H_2O molecule, while $\overset{\circ}{H}_{H_2O}(T)$ and $\overset{\circ}{S}_{H_2O}(T)$ are taken from thermodynamic tables.[15] The standard chemical potential, $\overset{\circ}{\mu}_{H_2O}$, is set to the calculated total electronic energy of the isolated H_2O molecule.

The contribution from phonons to the free energy, $F^{vib}(T)$ or $G^{vib}(T)$, and entropy, $S^{vib}(T)$, is in the harmonic approximation given by

$$F^{vib}(T) = \frac{1}{2}\sum_{\mathbf{q},s} h\nu(\mathbf{q},s) + k_B T \sum_{\mathbf{q},s} \ln\left(1 - \exp\left(-\frac{h\nu(\mathbf{q},s)}{k_B T}\right)\right) \tag{5}$$

$$S^{vib}(T) = -k_B \sum_{\mathbf{q},s} \ln\left(1 - \exp\left(-\frac{h\nu(\mathbf{q},s)}{k_B T}\right)\right) + \frac{1}{T}\sum_{\mathbf{q},s} \frac{h\nu(\mathbf{q},s)}{\exp\left(\frac{h\nu(\mathbf{q},s)}{k_B T}\right) - 1} \tag{6}$$

where $\nu(\mathbf{q},s)$ are the phonon frequencies throughout the $\mathbf{q}$-space. Although the vibrational frequencies in principle should be evaluated at all $\mathbf{q}$-points, the phonon spectra for the defective cells were only evaluated at the Γ-point of the defective supercells due to their large sizes. From eqn (6), the vibrational formation entropy of a defect is simply

$$\Delta_F S^{vib}_{defect} = S^{vib}_{defect}(T) - S^{vib}_{bulk}(T), \tag{7}$$

and similar for $\Delta_F H^{vib}_{defect}$, and $\Delta_F F^{vib}_{defect}$ or $\Delta_F G^{vib}_{defect}$. Note that we are assuming a negligible change in the thermal expansion coefficient upon defect formation, such that $\Delta_F S^{vib}_{defect}$ and $\Delta_F G^{vib}_{defect}$ calculated by full volume relaxations represent zero/constant pressure properties. We are currently also exploring anharmonic contributions to the defect formation entropies and thermal expansion of $BaCeO_3$ in more detail, which indicate that these contributions are of minor importance for the defect thermodynamics of $BaCeO_3$.

2.2 Hydration thermodynamics

The enthalpy and entropy of hydration according to eqn (1) can readily be determined from eqn (3)–(7):

$$\Delta_{Hydr}H^\circ = 2\Delta_F \overset{\circ}{H}_{OH^\bullet_O} - \Delta_F \overset{\circ}{H}_{v^{\bullet\bullet}_O} = 2\left(\Delta E^{el}_{OH^\bullet_O} + \Delta\varepsilon_{OH^\bullet_O} + \Delta_F H^{vib}_{OH^\bullet_O}\right) - \left(\Delta E^{el}_{v^{\bullet\bullet}_O} + 2\Delta\varepsilon_{v^{\bullet\bullet}_O} + \Delta_F H^{vib}_{v^{\bullet\bullet}_O}\right) - \left(\overset{\circ}{\mu}_{H_2O} + H^{zp}_{H_2O} + \overset{\circ}{H}_{H_2O}(T)\right) \tag{8}$$

$$\Delta_{Hydr}S^\circ = 2\Delta_F S^{vib}_{OH^\bullet_O} - \Delta_F S^{vib}_{v^{\bullet\bullet}_O} - \overset{\circ}{S}_{H_2O}(T) \tag{9}$$

Upon experimental determination of $\Delta_{Hydr}S^\circ$ by curve fitting of eqn (2) to *e.g.* water uptake data from thermogravimetric measurements, it is usually assumed that the number of regular positions for $OH^\bullet_O$ and $v^{\bullet\bullet}_O$ equal the number of oxide ions per formula unit.[2] For perovskites, $OH^\bullet_O$ is normally found to take on a number of different configurations around each oxide ion, depending on the crystal structure. Further, in oxides where $v^{\bullet\bullet}_O$ preferentially forms on one of the several structurally distinct oxide ions, the number of regular positions for $v^{\bullet\bullet}_O$ is lower than the concentration of O lattice sites. The number of proton positions (N_H) around each oxide ion and the number of vacancy configurations (N_v) affect the chemical potential of $OH^\bullet_O$

and $v_O^{\bullet\bullet}$, and thus K_{Hydr}. Not accounting for these configurations when evaluating defect thermodynamics by curve fitting results in an apparent hydration entropy, $\Delta_{Hydr}S^{\circ}_{app}$, which, in addition to the vibrational contributions, also includes configurational contributions:

$$\Delta_{Hydr}S^{\circ}_{app} = \Delta_{Hydr}S^{\circ} + \Delta_{Hydr}S^{conf}_{app} = \Delta_{Hydr}S^{\circ} - 2R\sum_{i}^{N_H} p_{i,H}\ln(N_O p_{i,H}) + R\sum_{i}^{N_v} p_{i,v}\ln(N_O p_{i,v}) \quad (10)$$

N_O is the number of oxide ions per formula unit, while $p_{i,H}$ and $p_{i,v}$ are the conditional probabilities for occupation of each configuration at an oxide ion by $OH_O^{\bullet}$ and $v_O^{\bullet\bullet}$, respectively. The general expression for the probability of occupation of a given configuration is for instance for the proton given by

$$p_{i,H} = \frac{\exp(-E_i/k_B T)}{\sum_{i}^{N_H}\exp(-E_i/k_B T)} \quad (11)$$

where E_i are the relative energies of the different N_H configurations around the N_O oxide ions (3 for perovskites). It is important to note that $\Delta_{Hydr}S^{conf}_{app}$ in eqn (10) only accounts for the configurational contributions stemming from distributing a proton or an oxygen vacancy over N_H and N_v configurations at one specific oxide ion, as the remaining contributions are accounted for through the mass action law (eqn (2)). At higher temperatures or in perovskites where the different N_H and N_v are degenerate, eqn (10) converges to

$$\Delta_{Hydr}S^{\circ}_{app} = \Delta_{Hydr}S^{\circ} + 2R\ln(N_H) \quad (12)$$

3 Computational details

The first principles calculations are performed with the plane-wave Density Functional Theory (DFT) approach within the VASP (v.5.3.5) code,[16,17] at the GGA-PBE[18] and/or LDA[19] level with a constant plane-wave cut-off energy of 500 eV. For the cubic $BaZrO_3$ and $BaSnO_3$, all defect calculations were performed with $3 \times 3 \times 3$ (135 atoms) supercell expansions, while $2 \times 2 \times 2$ supercells (160 atoms) were used for orthorhombic $BaCeO_3$ and $SrZrO_3$. Electronic integration was performed using a $2 \times 2 \times 2$ Monkhorst-Pack **k**-mesh over the supercell. Further, all calculations were performed using a reciprocal projection scheme, with ionic and electronic convergence criteria of 10^{-4} eV Å^{-1} and 10^{-8} eV, respectively. The number of electrons in the supercell was adjusted to simulate the desired charge state of the defects, which was compensated by a homogeneous, opposite background charge. Finally, the defect calculations were performed both by fixing the volume to that of the defect-free bulk, or by relaxing both the supercell shape and its volume, in order to simulate constant volume, or zero/constant pressure conditions, respectively.

The phonon frequencies were calculated within the harmonic approximation using finite ionic displacements of ±0.01 Å. Fourier transform and diagonalisation of the dynamical matrix were performed using the phonopy code.[20,21] While $BaZrO_3$, $BaCeO_3$ and $SrZrO_3$ displayed no imaginary modes, $BaSnO_3$ exhibited imaginary modes at the *R*-point of the Brillouin zone with the GGA-PBE functional. With the LDA functional however, all modes of $BaSnO_3$ were found to be positive and this functional was therefore chosen to avoid erroneous contributions to the vibrational thermodynamics. All electronic contributions to the defect thermodynamics were, however, evaluated with the GGA-PBE functional – for consistency.

Table 2 shows the calculated lattice parameters and unit cell volumes of the four included perovskites. As is typically observed, GGA consistently overestimates the lattice parameters slightly, while the LDA parameters for $BaSnO_3$ are somewhat underestimated.

4 Results and discussion

4.1 Site degeneracy and configurational entropy

The orientation of the protonic defect around each oxide ion has previously been shown to depend on the symmetry of the structure, but also on the lattice constant/volume of the unit cell.[26] In $BaZrO_3$, $BaSnO_3$, $BaCeO_3$ and $SrZrO_3$, the proton takes on a position along the bisector of two O connecting lines and there are thus 4 proton positions per oxide ion.[26–30] While these positions are degenerate in $BaZrO_3$ and $BaSnO_3$, they are non-degenerate in the orthorhombic $BaCeO_3$ and $SrZrO_3$. In the denser $SrTiO_3$, on the other hand, protons have been argued to take on a position along the edge of the TiO_6 polyhedra, resulting in 8 equivalent positions around each oxide ion.[31,32] Our calculations are in general agreement with those of refs 26–30 showing that all included compositions exhibit proton positions at, or close to, the bisector of two oxygen connecting lines (see Fig. 1). The site is 4-fold degenerate in $BaZrO_3$ and $BaSnO_3$, while $BaCeO_3$ and $SrZrO_3$ display 4 unique minima around each of the O1 and O2 ions within 0.20 and 0.18 eV of

Table 2 Calculated lattice parameters and unit cell volumes (per f.u.) for $BaZrO_3$, $BaSnO_3$, $BaCeO_3$ and $SrZrO_3$. For $BaSnO_3$, the results refer to calculations with the LDA functional, while the GGA results are given in parentheses

	$BaZrO_3$		$BaSnO_3$		$BaCeO_3$		$SrZrO_3$	
	DFT	Exp.[22]	DFT	Exp.[23]	DFT	Exp.[24]	DFT	Exp.[25]
a (Å)	4.236	4.19	4.096 (4.188)	4.118	6.289	6.235	5.859	5.815
b (Å)	—		—		8.865	8.781	8.254	8.196
c (Å)	—		—		6.286	6.212	5.819	5.786
V (Å^3)	75.96	73.6	68.74 (73.44)	69.83	87.62	85.03	70.83	68.94

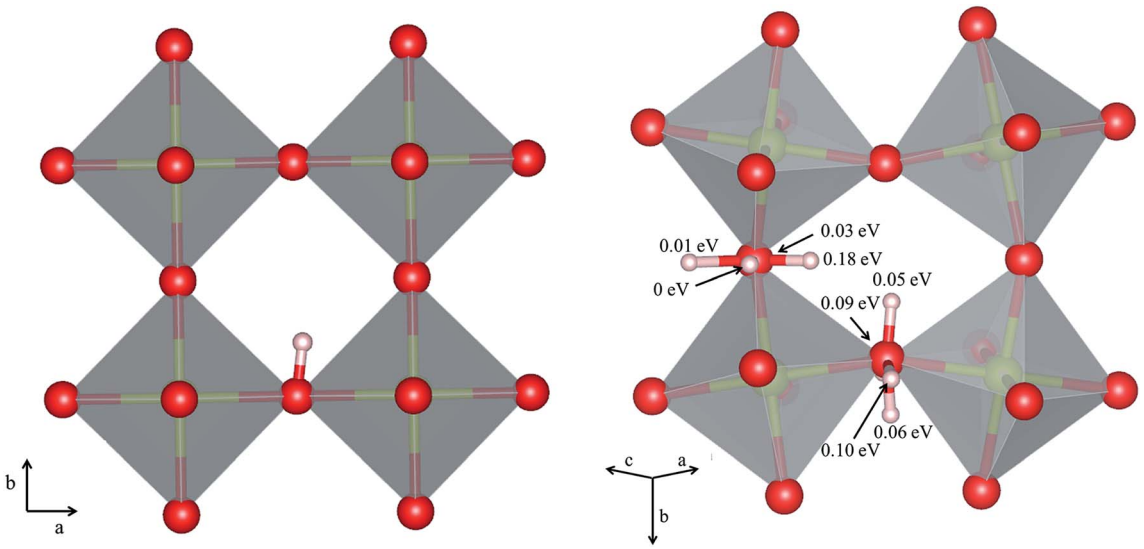

Fig. 1 Proton positions in (left) $BaZrO_3$ and (right) $SrZrO_3$ with *b* as the apical axis. For $SrZrO_3$ we also report the stability (in eV) of the different configurations relative to the most stable configuration around the O1 ion.

each other, respectively (*cf.* Fig. 1 for $SrZrO_3$). In $BaCeO_3$ and $SrZrO_3$, we also find that $v_O^{\bullet\bullet}$ is favoured by merely 70 and 60 meV, for $BaCeO_3$ and $SrZrO_3$, respectively, at the O1 compared to the O2 site. As shown in Fig. 2, the non-degenerate proton and oxygen vacancy configurations in $SrZrO_3$ and $BaCeO_3$ render the configurational contribution to the hydration entropy temperature dependent. At the lowest temperatures, the contribution is actually negative due to the preference for occupation of the O1 site by oxygen vacancies. However, due to the small energy difference between the various proton and oxygen vacancy configurations, the configurational contribution approaches that for $BaZrO_3$ even at ~600 K. Both $SrZrO_3$ and $BaCeO_3$ also undergo several phase transitions upon heating, which may affect the relative stability of the different proton and vacancy configurations. Hence, the configurational contribution to $\Delta_{Hydr}S^\circ$ is approximately $2R\ln(4)$ (23 J K^{-1} mol^{-1}) within the majority of the experimental temperature window (600–1100 K) for all included perovskites. Any compositional dependence of $\Delta_{Hydr}S^\circ$, in contrast to the conclusions of Tauer *et al.*,[33] is therefore of a purely vibrational nature, and will be the focus in the remaining parts of this contribution.

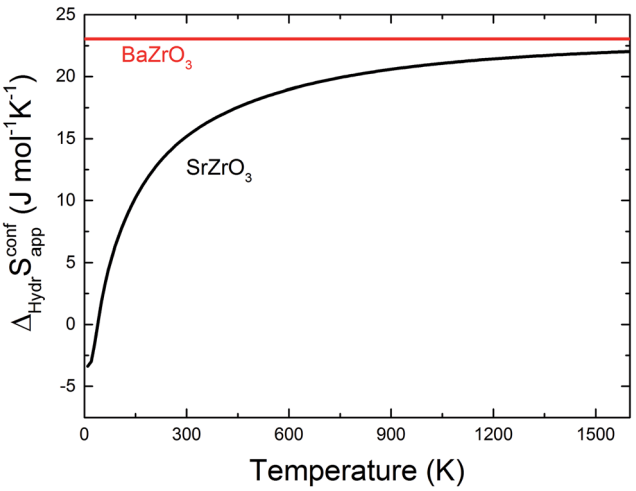

Fig. 2 Configurational contribution to $\Delta_{Hydr}S^\circ$ when neglecting the site degeneracy of protons and oxygen vacancies ($\Delta_{Hydr}S^{conf}_{app}$) of $BaZrO_3$ and $SrZrO_3$ as a function of temperature according to eqn (10).

4.2 Chemical expansion

In our previous contribution on $BaZrO_3$,[10] the formation volume of a defect was shown to have major implications for its formation entropy under zero/constant pressure conditions. In addition, the formation volume determines the chemical expansion coefficient of defects, and thus also the chemical expansion of the material upon *e.g.* hydration (eqn (1)).

The normalised volumetric chemical expansion coefficient, ε_i, of a defect *i* is here taken as:[34]

$$\varepsilon_i = \frac{1}{\delta}\left(\frac{V_i}{V_0} - 1\right) \quad (13)$$

where V_i and V_0 are the volumes of the defective and perfect supercells, respectively, while δ is the defect concentration in mole fractions (1/27 for $BaZrO_3$ and $BaSnO_3$, and 1/32 for $BaCeO_3$ and $SrZrO_3$). Correspondingly, the chemical expansion upon hydration (eqn (1)) may be quantified through

$$\varepsilon_{Hydr} = 2\varepsilon_{OH_O^\bullet} - \varepsilon_{v_O^{\bullet\bullet}} \quad (14)$$

where $\varepsilon_{OH_O^\bullet}$ and $\varepsilon_{v_O^{\bullet\bullet}}$ are the chemical expansion coefficients of $OH_O^\bullet$ and $v_O^{\bullet\bullet}$, respectively. ε_{Hydr} is thus given as the relative expansion upon hydration of 1 mole of $v_O^{\bullet\bullet}$, and with respect to the volume of the *defect-free lattice*. Experimentally, however, chemical expansion coefficients are taken as the relative volume of the hydrated and dry materials – *i.e.* relative to the *defective lattice*. Experimental ε_{Hydr} will therefore appear somewhat larger than those determined computationally in this work and in *e.g.* ref. 34.

Table 3 Linear (ε_a, ε_b, ε_c) and volumetric (ε_i) chemical expansion coefficients, formation volumes ($\Delta_F V_i$), of $OH_O^\bullet$ and $v_O^{\bullet\bullet}$, and chemical expansion coefficient upon hydration (ε_{Hydr}) for the included perovskites. The $v_O^{\bullet\bullet}$ in $BaZrO_3$ and $BaSnO_3$ is aligned with the Zr(Sn)-$v_O^{\bullet\bullet}$-Zr(Sn) axis parallel to the a-axis, while in $BaCeO_3$ and $SrZrO_3$ it is parallel to the b-axis. Note that the calculations on $BaSnO_3$ are performed with the LDA functional

	$BaZrO_3$		$BaSnO_3$		$BaCeO_3$		$SrZrO_3$	
	$OH_O^\bullet$	$v_O^{\bullet\bullet}$	$OH_O^\bullet$	$v_O^{\bullet\bullet}$	$OH_O^\bullet$	$v_O^{\bullet\bullet}$	$OH_O^\bullet$	$v_O^{\bullet\bullet}$
$\varepsilon_{i,a}$	0.0158	−0.0496	0.007	−0.0379	−0.0475	−0.1111	−0.0463	−0.1176
$\varepsilon_{i,b}$	−0.0566	−0.0952	−0.0540	−0.0973	−0.0429	−0.0688	−0.0110	−0.0323
$\varepsilon_{i,c}$	−0.0178	−0.0952	−0.0138	−0.0973	0.0238	−0.0454	−0.0116	−0.0560
$\Delta_F V_i$	−4.44 Å^3	−18.1 Å^3	−4.14 Å^3	−15.9 Å^3	−5.86 Å^3	−19.7 Å^3	−4.87 Å^3	−14.6 Å^3
ε_i	−0.0587	−0.239	−0.060	−0.232	−0.067	−0.225	−0.069	−0.206
ε_{Hydr}	0.122		0.111		0.0911		0.068	
ε_{Hydr}^{Exp}	0.160 (In doped),[37] 0.176 (Y doped),[6] 0.115–0.227 (Y doped)[38]		—		0.030–0.099 (Yb doped),[39] 0.151 (Y doped)[38]		—	

Table 3 shows the calculated chemical expansion coefficients and formation volumes of $OH_O^\bullet$ and $v_O^{\bullet\bullet}$ (both linear and volumetric), along with the chemical expansion upon hydration. All expansion coefficients are given per mole of formed defect. Both defects lead to anisotropic relaxations of the supercell for the four perovskites, even for the cubic $BaZrO_3$ and $BaSnO_3$, where $v_O^{\bullet\bullet}$ leads to a tetragonal cell, in line with experimental reports.[7,35,36] For all compositions, both defects display negative formation volumes and are thus smaller than the native oxide ions, with $v_O^{\bullet\bullet}$ leading to a considerably larger contraction than $OH_O^\bullet$. $\varepsilon_{v_O^{\bullet\bullet}}$ increases (less negative) notably in the order $BaZrO_3$ → $BaSnO_3$ → $BaCeO_3$ → $SrZrO_3$, while $\varepsilon_{OH_O^\bullet}$ follows the opposite trend. The calculated ε_{Hydr} are comparable with the experimentally determined values, although the experimental values vary considerably with the dopant concentration, and the adopted method (which most likely originates from uncertain proton concentrations). Hence, the compositional dependence of ε_{Hydr} is somewhat unclear from the experimental values. Our calculated ε_{Hydr} on the other hand decreases notably in the order $BaZrO_3$ → $BaSnO_3$ → $BaCeO_3$ → $SrZrO_3$, which stems from both the decreasing $\varepsilon_{OH_O^\bullet}$ and the increasing $\varepsilon_{v_O^{\bullet\bullet}}$. Interestingly, these results therefore indicate that issues associated with the chemical expansion of $BaZrO_3$ electrolytes upon hydration may for instance be reduced by adopting $BaZrO_3$–$BaCeO_3$ solid solutions.

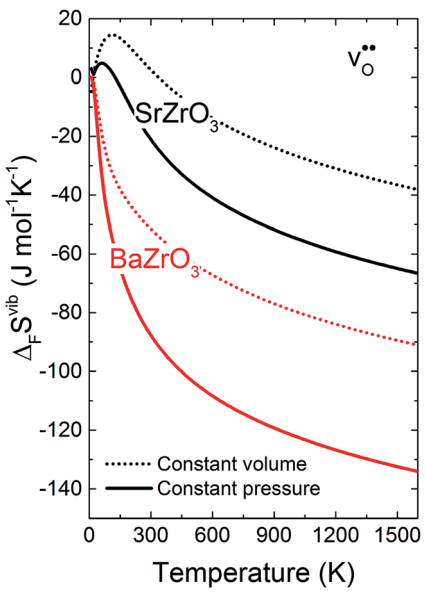

Fig. 3 $\Delta_F S_{v_O^{\bullet\bullet}}^{vib}$ of $SrZrO_3$ and $BaZrO_3$ calculated under constant volume or zero/constant pressure (*i.e.*, relaxed volume) conditions.

4.3 Defect entropies

Fig. 3 shows the vibrational contribution to the formation entropy ($\Delta_F S_{v_O^{\bullet\bullet}}^{vib}$) of $v_O^{\bullet\bullet}$ in $SrZrO_3$ and $BaZrO_3$ calculated under constant volume and zero/constant pressure conditions. For both compounds, $\Delta_F S_{v_O^{\bullet\bullet}}^{vib}$ is negative, and significantly more negative under zero/constant pressure than under constant volume conditions – which stems from a blue shift of the phonon spectrum due to the negative formation volume of $v_O^{\bullet\bullet}$.[10] Further, the effect is more noticeable for $BaZrO_3$ than for $SrZrO_3$, in line with the more negative formation volume of $v_O^{\bullet\bullet}$ in $BaZrO_3$. Similar effects of volume relaxation on $\Delta_F S_{v_O^{\bullet\bullet}}^{vib}$ were also found for $BaSnO_3$ and $BaCeO_3$.

Fig. 4 shows $\Delta_F S_{OH_O^\bullet}^{vib}$ and $\Delta_F S_{v_O^{\bullet\bullet}}^{vib}$ for the four included perovskites, calculated under zero/constant pressure conditions. For all compositions, $\Delta_F S_{v_O^{\bullet\bullet}}^{vib}$ is significantly more negative than $\Delta_F S_{OH_O^\bullet}^{vib}$, and also shows a stronger compositional dependence. While all $\Delta_F S_{OH_O^\bullet}^{vib}$ fall within 15 J mol^{-1} K^{-1} of each other throughout the temperature interval, $\Delta_F S_{v_O^{\bullet\bullet}}^{vib}$ differs by as much as 80 J mol^{-1} K^{-1} at 1000 K between $BaZrO_3$ and $SrZrO_3$. The compositional variation of $\Delta_F S_{v_O^{\bullet\bullet}}^{vib}$ to some extent follows $\varepsilon_{v_O^{\bullet\bullet}}$, with the two cubic perovskites, $BaZrO_3$ and $BaSnO_3$, displaying significantly more negative entropies than the orthorhombic $SrZrO_3$ and $BaCeO_3$. Hence, the compositional dependence of $\Delta_F S_{v_O^{\bullet\bullet}}^{vib}$ partly stems from the changes in $\varepsilon_{v_O^{\bullet\bullet}}$ through the series, and partly from varying local structural relaxations around the defect (as reflected by the compositional dependence of $\Delta_F S_{v_O^{\bullet\bullet}}^{vib}$ under constant volume conditions, see Fig. 3).

4.4 Hydration thermodynamics

Fig. 5 compares the calculated enthalpies (a) and entropies (b) of hydration according to eqn (1) for $BaZrO_3$, $BaSnO_3$, $SrZrO_3$ and $BaCeO_3$. Interestingly, the vibrational contribution to

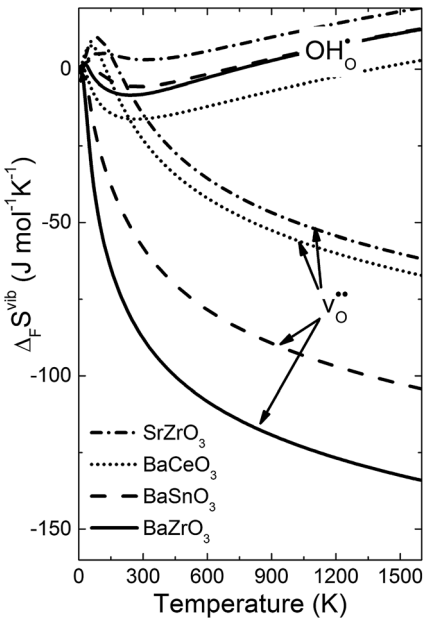

Fig. 4 Calculated $\Delta_F S^{vib}_{OH^{\bullet}_O}$ and $\Delta_F S^{vib}_{V^{\bullet\bullet}_O}$ for the four included perovskites calculated under zero/constant pressure conditions.

$\Delta_{Hydr}H^\circ$ results in a slight temperature dependence, and $\Delta_{Hydr}H^\circ$ therefore becomes less negative with increasing temperature for all compositions. Experimentally, $\Delta_{Hydr}H^\circ$ is determined from eqn (2) over a wide temperature interval such that the temperature dependence of $\Delta_{Hydr}H^\circ$ (and $\Delta_{Hydr}S^\circ$) is not observed. In a recent work,[3] we indicated, from combined thermogravimetric measurements of water uptake and differential scanning calorimetry (TG-DSC), that $\Delta_{Hydr}H^\circ$ of Sc and In doped $BaTiO_3$ actually displays weak temperature dependencies in accordance with Fig. 5. The experimentally determined $\Delta_{Hydr}H^\circ$ and $\Delta_{Hydr}S^\circ$ listed in Table 1 should therefore be compared with the temperature averaged $\Delta_{Hydr}\bar{H}^\circ$ and $\Delta_{Hydr}\bar{S}^\circ$ from linearisation of the computational $\Delta_{Hydr}G^\circ$ *vs.* T (see Table 4). For comparative reasons, $\Delta_{Hydr}\bar{S}^\circ_{app}$ values in Table 4 represent the temperature averaged apparent entropy of hydration,

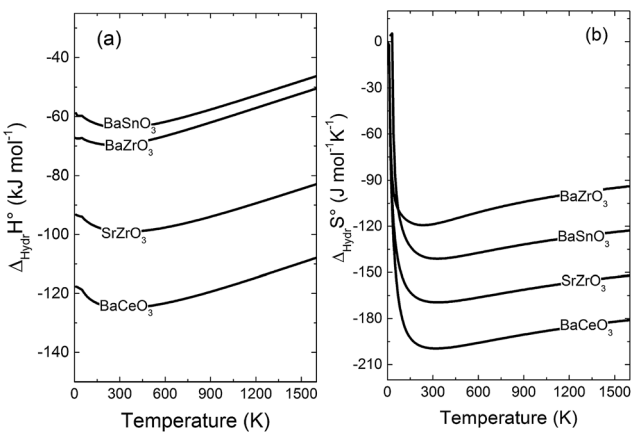

Fig. 5 Calculated (a) enthalpy and (b) entropy of hydration of $BaZrO_3$, $BaSnO_3$, $SrZrO_3$ and $BaCeO_3$.

Table 4 Temperature averaged standard hydration enthalpy and entropy of $BaZrO_3$, $BaSnO_3$, $SrZrO_3$ and $BaCeO_3$. For consistency with experimental values, a constant configurational contribution of 23 J mol^{-1} K^{-1} to $\Delta_{Hydr}\bar{S}^\circ$ has been included for all compositions

	$\Delta_{Hydr}\bar{H}^\circ$ (kJ mol^{-1})	$\Delta_{Hydr}\bar{S}^\circ_{app}$ (J mol^{-1} K^{-1})
$BaZrO_3$	−65	−84
$BaSnO_3$	−60	−109
$SrZrO_3$	−97	−141
$BaCeO_3$	−122	−171

i.e. including the configurational contribution according to eqn (11) (23 J mol^{-1} K^{-1} for all compositions).

The $\Delta_{Hydr}\bar{H}^\circ$ values are, as expected, very close to the low temperature $\Delta_{Hydr}H^\circ$ in Fig. 5, and are in reasonable agreement with the experimental ranges of enthalpies for all compositions in Table 1. The calculated values also reflect the experimentally observed compositional dependence, with the two cubic perovskites displaying significantly less exothermic enthalpies than the two orthorhombic members. Also the calculated $\Delta_{Hydr}\bar{S}^\circ$ values are in good agreement with the experimental values in Table 1. The entropies display a distinct compositional dependence, and are in general less negative for the cubic $BaZrO_3$ and $BaSnO_3$ than for the orthorhombic $SrZrO_3$ and $BaCeO_3$. The less negative $\Delta_{Hydr}S^\circ$ of $BaZrO_3$ and $BaSnO_3$ stabilises protons compared to in the orthorhombic $BaCeO_3$ and $SrZrO_3$, in line with Kreuer's remark that the favourable proton transport properties of $BaZrO_3$ stems from entropic stabilisation of protons.[6] As noted in Fig. 3, $\Delta_F S^{vib}_{V^{\bullet\bullet}_O}$ is the dominant vibrational contribution to $\Delta_{Hydr}S^\circ$, and also shows a stronger compositional dependency than $\Delta_F S^{vib}_{OH^{\bullet}_O}$. Hence, one may argue that the entropic stabilisation of protons in $BaZrO_3$/$BaSnO_3$ is, more precisely, a result of entropic *destabilisation* of $V^{\bullet\bullet}_O$.

Turning to the hydration enthalpy, the strong compositional dependency (*cf.* Table 4) is generally in line with experimental observations; orthorhombic perovskites exhibit more exothermic values than the cubic, *i.e.* it becomes more exothermic with a decreasing electronegativity difference between the B- and A-site cations, but also with a decreasing Goldschmidt tolerance factor.[8,9] These correlations are usually attributed to the basicity/ionicity of the oxide, which affects the bonding strength of $V^{\bullet\bullet}_O$ and $OH^{\bullet}_O$; the oxide with the most exothermic hydration enthalpies exhibits the most stable protonic defects, and the most unstable oxygen vacancies (*i.e.* most stable oxide ions). There is further a striking correlation between both the calculated and experimental $\Delta_{Hydr}\bar{H}^\circ$ and $\Delta_{Hydr}\bar{S}^\circ$ values, with the compound displaying the most exothermic $\Delta_{Hydr}\bar{H}^\circ$ ($BaCeO_3$) also displaying the most negative (least favorable) $\Delta_{Hydr}\bar{S}^\circ$. The correlation between $\Delta_{Hydr}\bar{H}^\circ$ and $\Delta_{Hydr}\bar{S}^\circ$ is far from intuitive since $\Delta_{Hydr}\bar{S}^\circ$ depends on both $\Delta_F S^{vib}_{OH^{\bullet}_O}$ and $\Delta_F S^{vib}_{V^{\bullet\bullet}_O}$, neither of which correlate directly with either $\varepsilon_{V^{\bullet\bullet}_O}$, $\varepsilon_{OH^{\bullet}_O}$ or ε_{Hydr}, or the volume of the unit cells, as one might expect. The contributions to $\Delta_F S^{vib}_{OH^{\bullet}_O}$ and $\Delta_F S^{vib}_{V^{\bullet\bullet}_O}$ are related to both the vibrational frequency of protons and oxide ions, local relaxations upon protonation and filling of the $V^{\bullet\bullet}_O$, in addition to the chemical expansion of the unit cell upon

hydration. These properties can again be related to the size of the cations in the perovskite structure (which determines the unit cell volume and symmetry), and their electronegativity (which determines the interatomic bonding strengths), which – somewhat speculatively – explains the observed correlation between $\Delta_{Hydr}\bar{H}^\circ$ and $\Delta_{Hydr}\bar{S}^\circ$. Conclusively, the oxide exhibiting the most stable protons and least stable vacancies enthalpy-wise, also exhibits weaker entropic destabilisation of vacancies, and thus the least favourable entropies of hydration.

5 Conclusions

We have in this work assessed the thermodynamics of hydration, with emphasis on vibrational contributions, and the chemical expansion of the four proton conducting perovskites $BaZrO_3$, $BaSnO_3$, $BaCeO_3$ and $SrZrO_3$ from first principles phonon calculations. The calculations show that both $OH_O^\bullet$ and $v_O^{\bullet\bullet}$ are smaller than the native oxide ions in all materials. Further, $v_O^{\bullet\bullet}$ is significantly smaller than the proton and is therefore the main contributor to the chemical expansion of the materials upon hydration. The chemical expansion shows a distinct compositional dependence, and decreases in the order $BaZrO_3 \rightarrow BaSnO_3 \rightarrow BaCeO_3 \rightarrow SrZrO_3$. As such, proton conducting electrolytes composed of $BaZrO_3$–$BaCeO_3$ or $BaZrO_3$–$SrZrO_3$ solid solutions should be less prone to issues stemming from chemical expansion upon hydration than pure $BaZrO_3$ electrolytes. There is further a significant contribution from phonons to the formation entropy of both $OH_O^\bullet$ and $v_O^{\bullet\bullet}$. The contribution is most pronounced for $v_O^{\bullet\bullet}$, and negative for all compositions, and becomes less negative in the order $BaZrO_3 \rightarrow BaSnO_3 \rightarrow BaCeO_3 \rightarrow SrZrO_3$, *i.e.* with increasing (less negative) chemical expansion of $v_O^{\bullet\bullet}$. Both the calculated $\Delta_{Hydr}H^\circ$ and $\Delta_{Hydr}S^\circ$ are in good agreement with the experimental ranges of values, and display a distinct compositional dependence. $\Delta_{Hydr}S^\circ$ is in general less negative (more favourable) for the cubic $BaZrO_3$ and $BaSnO_3$ than the orthorhombic members, reflecting its dependence on the vibrational formation entropy, and again the chemical expansion, of $v_O^{\bullet\bullet}$. Interestingly, there is a general correlation between $\Delta_{Hydr}H^\circ$ and $\Delta_{Hydr}S^\circ$; the two cubic members display the least exothermic $\Delta_{Hydr}H^\circ$, but also the least negative (and thus most favourable) $\Delta_{Hydr}S^\circ$ – an effect which may stem from both parameters being related to the bonding strengths of O^{2-} and H^+.

Acknowledgements

The authors gratefully acknowledge the Research Council of Norway (RCN), project "HydraThermPro" (project number 214252), and the Centre for Materials Science and Nanotechnology, for financial support. We also thank the Norwegian Metacenter for Computational Science (NOTUR) for computational resources and excellent support (project NN4604k).

References

1 H. Iwahara, T. Esaka, H. Uchida and N. Maeda, *Solid State Ionics*, 1981, **3–4**, 359–363.
2 K. D. Kreuer, *Solid State Ionics*, 1999, **125**, 285–302.
3 T. S. Bjørheim, S. M. H. Rahman, S. G. Eriksson, C. S. Knee and R. Haugsrud, *Inorg. Chem.*, 2015, **54**, 2858–2865.
4 C. Kjølseth, L.-Y. Wang, R. Haugsrud and T. Norby, *Solid State Ionics*, 2010, **181**, 1740–1745.
5 A. Løken, C. Kjølseth and R. Haugsrud, *Solid State Ionics*, 2014, **267**, 61–67.
6 K. D. Kreuer, *Annu. Rev. Mater. Res.*, 2003, **33**, 333–359.
7 K. D. Kreuer, S. Adams, W. Münch, A. Fuchs, U. Klock and J. Maier, *Solid State Ionics*, 2001, **145**, 295–306.
8 T. Norby, M. Widerøe, R. Glöckner and Y. Larring, *Dalton Trans.*, 2004, 3012–3018.
9 T. S. Bjørheim, A. Kuwabara, I. Ahmed, R. Haugsrud, S. Stølen and T. Norby, *Solid State Ionics*, 2010, **181**, 130–137.
10 T. S. Bjørheim, E. A. Kotomin and J. Maier, *J. Mater. Chem. A*, 2015, **3**, 7639–7648.
11 A. Løken, T. S. Bjørheim and R. Haugsrud, *J. Mater. Chem. A*, 2015, **3**, 23289–23298.
12 Y. Wang, A. Chesnaud, E. Bevillon and G. Dezanneau, *Solid State Ionics*, 2012, **214**, 45–55.
13 Y. Wang, A. Chesnaud, E. Bevillon, J. Yang and G. Dezanneau, *Int. J. Hydrogen Energy*, 2011, **36**, 7688–7695.
14 F. Krug and T. Schober, *J. Am. Ceram. Soc.*, 1997, **80**, 794–796.
15 M. W. Chase Jr, *Nist-janaf Thermochemical Tables*, The American Institute of Physics for The National Institute of Standards and Technology, New York, 4th edn, 1998.
16 G. Kresse and J. Furthmüller, *Phys. Rev. B: Condens. Matter Mater. Phys.*, 1996, **54**, 11169–11186.
17 G. Kresse and D. Joubert, *Phys. Rev. B: Condens. Matter Mater. Phys.*, 1999, **59**, 1758–1775.
18 J. P. Perdew, K. Burke and M. Ernzerhof, *Phys. Rev. Lett.*, 1996, **77**, 3865–3868.
19 D. M. Ceperley and B. J. Alder, *Phys. Rev. Lett.*, 1980, **45**, 566–569.
20 A. Togo, F. Oba and I. Tanaka, *Phys. Rev. B: Condens. Matter Mater. Phys.*, 2008, **78**, 134106.
21 A. Togo and I. Tanaka, *Scr. Mater.*, 2015, **108**, 1–5.
22 I. Levin, T. G. Amos, S. M. Bell, L. Farber, T. A. Vanderah, R. S. Roth and B. H. Toby, *J. Solid State Chem.*, 2003, **175**, 170–181.
23 E. Bévillon, A. Chesnaud, Y. Wang, G. Dezanneau and G. Geneste, *J. Phys.: Condens. Matter*, 2008, **20**, 145217.
24 A. J. Jacobson, B. C. Tofield and B. E. F. Fender, *Acta Crystallogr., Sect. B: Struct. Crystallogr. Cryst. Chem.*, 1972, **28**, 956–961.
25 A. Ahtee, M. Ahtee, A. M. Glazer and A. W. Hewat, *Acta Crystallogr., Sect. B: Struct. Crystallogr.Cryst. Chem.*, 1976, **32**, 3243–3246.
26 J. Hermet, M. Torrent, F. Bottin, G. Dezanneau and G. Geneste, *Phys. Rev. B: Condens. Matter Mater. Phys.*, 2013, **87**, 104303.
27 M. E. Björketun, P. G. Sundell and G. Wahnström, *Faraday Discuss.*, 2007, **134**, 247–265.
28 G. Geneste, A. Ottochian, J. Hermet and G. Dezanneau, *Phys. Chem. Chem. Phys.*, 2015, **17**, 19104–19118.
29 R. A. Davies, M. S. Islam and J. D. Gale, *Solid State Ionics*, 1999, **126**, 323–335.

30 R. Hempelmann, M. Soetratmo, O. Hartmann and R. Wäppling, *Solid State Ionics*, 1998, **107**, 269–280.
31 M. Cherry, M. S. Islam, J. D. Gale and C. R. A. Catlow, *J. Phys. Chem.*, 1995, **99**, 14614–14618.
32 E. Matsushita and T. Sasaki, *Solid State Ionics*, 1999, **125**, 31–37.
33 T. Tauer, R. O'Hayre and J. W. Medlin, *Solid State Ionics*, 2011, **204–205**, 27–34.
34 E. Jedvik, A. Lindman, M. Benediktsson and G. Wahnström, *Solid State Ionics*, 2015, **275**, 2–8.
35 K. D. Kreuer, *Annu. Rev. Mater. Res.*, 2003, **33**, 333–359.
36 F. Giannici, M. Shirpour, A. Longo, A. Martorana, R. Merkle and J. Maier, *Chem. Mater.*, 2011, **23**, 2994–3002.
37 F. G. Kinyanjui, S. T. Norberg, I. Ahmed, S. G. Eriksson and S. Hull, *Solid State Ionics*, 2012, **225**, 312–316.
38 A. K. E. Andersson, S. M. Selbach, C. S. Knee and T. Grande, *J. Am. Ceram. Soc.*, 2014, **97**, 2654–2661.
39 Y. Yamazaki, F. Blanc, Y. Okuyama, L. Buannic, J. C. Lucio-Vega, C. P. Grey and S. M. Haile, *Nat. Mater.*, 2013, **12**, 647–651.